Shell-model method for Gamow-Teller transitions in heavy deformed odd-mass nuclei

Long-Jun Wang,[1,2] Yang Sun,[1,3,4,5,*] and Surja K. Ghorui[1]

[1]*School of Physics and Astronomy, Shanghai Jiao Tong University, Shanghai 200240, China*
[2]*Department of Physics and Astronomy, University of North Carolina, Chapel Hill, North Carolina 27599-3255, USA*
[3]*Collaborative Innovation Center of IFSA, Shanghai Jiao Tong University, Shanghai 200240, China*
[4]*Institute of Modern Physics, Chinese Academy of Sciences, Lanzhou 730000, China*
[5]*China Institute of Atomic Energy, P.O. Box 275(10), Beijing 102413, China*

(Received 21 December 2017; published 4 April 2018)

A shell-model method for calculating Gamow-Teller (GT) transition rates in heavy deformed odd-mass nuclei is presented. The method is developed within the framework of the projected shell model. To implement the computation requirement when many multi-quasiparticle configurations are included in the basis, a numerical advancement based on the Pfaffian formula is introduced. With this new many-body technique, it becomes feasible to perform state-by-state calculations for the GT nuclear matrix elements of β-decay and electron-capture processes, including those at high excitation energies in heavy nuclei which are usually deformed. The first results, β^- decays of the well-deformed $A = 153$ neutron-rich nuclei, are shown as the example. The known $\log(ft)$ data corresponding to the $B(\mathrm{GT}^-)$ decay rates of the ground state of ^{153}Nd to the low-lying states of ^{153}Pm are well described. It is further shown that the $B(\mathrm{GT})$ distributions can have a strong dependence on the detailed microscopic structure of relevant states of both the parent and daughter nuclei.

DOI: 10.1103/PhysRevC.97.044302

I. INTRODUCTION

The knowledge of the weak interaction process is important not only for nuclear and particle physics but also for nuclear astrophysics [1–7]. On the one hand, β-decay and lepton-capture rates are indispensable nuclear inputs for understanding the s-, r-, and rp-process nucleosynthesis [8]. In particular, the Gamow-Teller (GT) rates, $B(\mathrm{GT})$, for highly excited states of medium-heavy and heavy nuclei are an important ingredient to model the late evolution of stars and the core-collapse supernovas [8–11]. On the other hand, to constrain the neutrino mass and solve the neutrino mass hierarchy in nuclear processes such as neutrinoless double-β decay, one needs to calculate the nuclear matrix elements of $B(\mathrm{GT})$ between the ground state of the parent and daughter nuclei as well as all low- and high-lying states of the intermediate nucleus as accurately as possible [12,13]. The majority of the above-mentioned quantities cannot be measured by any presently known experiments (although preliminary attempts have been made under very exotic experimental conditions [14,15]) and, therefore, theoretical calculations are crucial.

Experimentally, GT transitions can be studied by two kinds of methods: the traditional β-decay experiments and the modern charge-exchange (CE) reactions in the forward direction [16]. Although β-decay experiments have a simple physical mechanism and high energy resolution, the excitation energy of the study is limited, however, by the Q-value, which varies from less than 1 MeV close to the stability line to about 10 MeV when going far from the stability. The other limitation of β-decay experiments is that most nuclei undergo either β^+ or β^- decay but not both. For example, most neutron-rich nuclei could only undergo β^- decay, while electron captures of proton-rich nuclei in the β^+ direction are crucial for core-collapse supernova modeling. Charge-exchange reactions, however, could be used for extracting $B(\mathrm{GT})$ since they connect the same initial and final states as β decay [17]. CE reactions could make transitions both in the β^- direction, such as the (p, n), (^{3}He, t), and (^{6}Li, ^{6}He) reactions, and in the β^+ direction, such as the (n, p), $(d, {}^2\mathrm{He})$, $(t, {}^3\mathrm{He})$, and (^{7}Li, ^{7}Be) reactions. Another advantage of using CE to probe GT transition strengths is that it allows access to higher excitation energy since it is not limited by the Q-value. However, taking the CE reactions in the β^+ direction as an example, the (n, p) reaction, which has the simplest reaction mechanism, usually suffers from poor energy resolution ($\sim$1 MeV). The $(d, {}^2\mathrm{He})$ reaction can reach a resolution of 100–200 keV, but the reaction mechanism is complex and only a few examples from early experiments were reported [18,19]. Although the reaction mechanism of the $(t, {}^3\mathrm{He})$ reaction, with a resolution of 250–400 keV, has been well studied, it is still impossible to measure the GT strength of all states for many nuclei that are involved in nuclear networks. Therefore, despite the experimental advances, one has to rely heavily on theoretical calculations to obtain most of the GT strength distributions.

It has been widely suggested that the shell model is the preferable method for GT transition calculations for nuclear astrophysical purposes [8,10,20,21]. In fact, successful description of nuclear ground-state properties, energy spectra at moderate excitations, and electromagnetic and GT transitions among these states could be obtained by the state-of-the-art

*Corresponding author: sunyang@sjtu.edu.cn

shell-model diagonalization method. For example, the nuclear wave functions in the full sd-shell model space obtained by Wildenthal and Brown were applied to calculate the GT transition rates for the sd-shell nuclei [22–24]. Langanke and Martínez-Pinedo later made the shell-model GT rates available also for the pf-shell nuclei [25].

The conventional shell model, which diagonalizes the matrix of an effective Hamiltonian in a chosen model space spanned by the Slater determinants of valence nucleons, can treat explicitly two-body correlations among them. Despite its great success, problems still remain in modern shell-model calculations based on spherical bases. In many calculations, if the model space is spanned by a single harmonic-oscillator shell, the calculation of forbidden transitions is impossible since it must involve nuclear transitions between different parities corresponding to different major harmonic-oscillator shells. However, if multiple major shells are used, the number of the valence nucleons occupying the orbitals has to be severely restricted to avoid dimension explosion, which makes the application for arbitrarily heavy deformed systems unfeasible. Finally, shell-model calculations of GT transitions for highly excited nuclear states usually need to introduce approximations based on the Brink-Axel hypothesis [26], which has been found recently to be invalid at low and moderate initial excitation energy [11].

In the long history of the nuclear shell-model development, tremendous effort has been devoted to extending the shell-model capacity from its traditional territory to heavier shells. As it is impossible to treat an arbitrarily large nuclear system in a spherical shell-model framework, one is compelled to seek judicious schemes to deal with large nuclear systems. As discussed in depth in a recent review article [27], the central issue has been the shell-model truncation. There are many different ways of truncating a shell-model space. While in principle it does not matter how to prepare a model basis, it is crucial in practice to use the most efficient one. In this regard, we recognize the fact that, except for a few lying in the vicinity of shell closures, most nuclei in the nuclear chart are deformed. This naturally suggests for shell-model calculations to use a deformed basis to incorporate the physics in large systems. Using a deformed basis to perform shell-model calculations is the philosophy of the projected shell model (PSM) [28,29].

To compare with conventional spherical shell models, the PSM does not have the limitation in the size of nuclei to be applied. An initial attempt for the PSM to calculate GT transitions from even-even to odd-odd nuclei was reported in Ref. [30]. However, the need for a shell-model method for quantitative GT calculations for heavy deformed odd-mass nuclei is obvious. To take a recent example, there is an unsolved scientific question on the reactor antineutrino anomaly [31,32] found in the measurements of the neutrino-mixing angle θ_{13}, which has underscored the need to precisely understand the complete antineutrino spectra from fissioning systems. The crucial point is to calculate antineutrino spectra for the fuels of commercial nuclear reactors, contributed by many individual nuclides in the fission products. As pointed out in Ref. [33], the decay from odd-Z and odd-N nuclides represents about 50% of this quantity. Hence, precise knowledge about the β-decay rate of these odd-mass nuclei is enormously important for the concerns of the nuclear physics problem in reactor neutrino physics.

Before a detailed presentation of the present work, let us update a few attractive features in the PSM approach, which may be relevant to future nuclear structure and astrophysical applications.

(i) The PSM adopts deformed mean -fields as its basis to construct many-body wave functions in which shell-model diagonalization is carried out. Therefore, the PSM bridges the two important nuclear structure models, the deformed mean-field approach and the conventional shell model, and takes the advantage of both. On the one hand, as a shell-model method, the PSM can be employed to study any (super)heavy (super)deformed nuclei without a size limitation. On the other hand, unlike the usual mean-field models, the PSM wave functions contain correlations beyond mean field and the states are written in the laboratory frame having, in principle, definite quantum numbers such as angular momentum, particle number, and parity.

(ii) Since the PSM states are defined in the (projected) deformed bases, the dimension of the configuration space in which the Hamiltonian is diagonalized is usually small (typically about 10^2–10^4). Therefore, state-by-state evaluations of nuclear matrix elements for GT transition are computationally feasible even for heavy deformed nuclei. In addition, as we show later, GT transitions for highly excited states can be calculated directly by employing the modern Pfaffian algorithm [34–38]. Approximations using the Brink-Axel hypothesis, which were widely used in shell-model calculations but for which the general validity has not been seriously questioned [11], are not needed here. This feature is important because GT transition rates of highly excited states of heavy nuclei are crucial nuclear inputs for many astrophysical processes.

(iii) Forbidden transitions involve nuclear orbits of different harmonic-oscillator shells and thus require multi-shell model spaces. Such calculations are not feasible for most of the conventional shell models working in one-major-shell bases. The PSM is a multishell shell model. This feature is desired particularly when, in some processes, forbidden transitions dominate. A recent work on the stellar origin of the ^{182}Hf cosmochronometer [39] represents an example of such a requirement.

(iv) Nuclear isomeric states play special roles in nuclear physics and astrophysics [40]. The relatively long half-lives of these isomers could change significantly the elemental abundances produced in nucleosynthesis. In some cases, an isomer with a long lifetime can change the paths of reaction and lead to a different set of elemental abundances [41]. The PSM has been shown to be capable of describing nuclear isomers well [37,42].

The aim of the present work is to extend the early work by Gao, Sun, and Chen [30], where GT transitions for even-mass

systems were discussed, to heavy deformed odd-A systems. A workable computer code has been developed with help of the Pfaffian formulas. The paper is organized as follows. In Sec. II, we introduce briefly the general formalism of the PSM for the calculation of the GT transition. The spectra of ^{153}Nd and ^{153}Pm and the Gamow-Teller transition strengths for the β^- decay between them are discussed in Sec. III. Finally, the paper is summarized and an outlook on future applications and developments is given in Sec. IV.

II. THEORETICAL FRAMEWORK AND NUMERICAL ALGORITHM

A. Wave function in the projected basis

The PSM employs the deformed Nilsson model [43] to generate a single-particle basis. Pairing correlations are considered by a BCS calculation. The Nilsson-BCS calculation defines a deformed quasiparticle (qp) basis from which the PSM space is constructed [27,28]. Three (four) major harmonic-oscillator shells are usually taken into account in calculations of heavy (superheavy and superdeformed) nuclei for both neutrons and protons. Let us use $a^\dagger_\nu$,$a^\dagger_\pi$ (a_ν,a_π) to denote neutron and proton qp creation (annihilation) operators associated with the qp vacuum $|\Phi\rangle$. The current coding includes multi-qp configurations up to seven-qp states for odd-neutron nuclei,

$$\{a^\dagger_{\nu_i}|\Phi\rangle,\ a^\dagger_{\nu_i}a^\dagger_{\nu_j}a^\dagger_{\nu_k}|\Phi\rangle,\ a^\dagger_{\nu_i}a^\dagger_{\pi_j}a^\dagger_{\pi_k}|\Phi\rangle,\ a^\dagger_{\nu_i}a^\dagger_{\nu_j}a^\dagger_{\nu_k}a^\dagger_{\pi_l}a^\dagger_{\pi_m}|\Phi\rangle,$$
$$a^\dagger_{\nu_i}a^\dagger_{\nu_j}a^\dagger_{\nu_k}a^\dagger_{\nu_l}a^\dagger_{\nu_m}a^\dagger_{\pi_n}a^\dagger_{\pi_o}|\Phi\rangle,\ a^\dagger_{\nu_i}a^\dagger_{\nu_j}a^\dagger_{\nu_k}a^\dagger_{\pi_l}a^\dagger_{\pi_m}a^\dagger_{\pi_n}a^\dagger_{\pi_o}|\Phi\rangle\}, \tag{1}$$

and for odd-proton nuclei,

$$\{a^\dagger_{\pi_i}|\Phi\rangle,\ a^\dagger_{\pi_i}a^\dagger_{\pi_j}a^\dagger_{\pi_k}|\Phi\rangle,\ a^\dagger_{\pi_i}a^\dagger_{\nu_j}a^\dagger_{\nu_k}|\Phi\rangle,\ a^\dagger_{\pi_i}a^\dagger_{\pi_j}a^\dagger_{\pi_k}a^\dagger_{\nu_l}a^\dagger_{\nu_m}|\Phi\rangle,$$
$$a^\dagger_{\pi_i}a^\dagger_{\pi_j}a^\dagger_{\pi_k}a^\dagger_{\pi_l}a^\dagger_{\pi_m}a^\dagger_{\nu_n}a^\dagger_{\nu_o}|\Phi\rangle,\ a^\dagger_{\pi_i}a^\dagger_{\pi_j}a^\dagger_{\pi_k}a^\dagger_{\nu_l}a^\dagger_{\nu_m}a^\dagger_{\nu_n}a^\dagger_{\nu_o}|\Phi\rangle\}. \tag{2}$$

We emphasize that the PSM works with multiple harmonic-oscillator shells for both neutrons and protons in the basis. That is to say, the indices ν (for neutrons) and π (for protons) in Eqs. (1) and (2) are general, and the configurations in Eqs. (1) and (2) can belong either to a positive- or to a negative-parity state. Thus the coding has been prepared for later applications for highly excited states with GT calculations.

The PSM wave function is a linear combination of projected states,

$$\left|\Psi^\omega_{\rm IM}\right\rangle = \sum_{K\kappa} f^\omega_{IK_\kappa}\hat{P}^I_{\rm MK}|\Phi_\kappa\rangle, \tag{3}$$

with definite angular momentum and parity, where $|\Phi_\kappa\rangle$ are the qp states in Eqs. (1) and (2). $\hat{P}^I_{\rm MK}$ is the angular momentum projection operator [44],

$$\hat{P}^I_{\rm MK} = \frac{2I+1}{8\pi^2}\int d\Omega D^I_{\rm MK}(\Omega)\hat{R}(\Omega), \tag{4}$$

with $D^I_{\rm MK}$ being the D function [45], $\hat{R}$ the rotation operator, and Ω the Euler angle. The energies and wave functions are obtained by solving the eigenvalue equation:

$$\sum_{K'\kappa'}\left(H^I_{K\kappa,K'\kappa'} - E^\omega_I N^I_{K\kappa,K'\kappa'}\right)f^\omega_{IK'_{\kappa'}} = 0, \tag{5}$$

where $H^I_{K\kappa,K'\kappa'}$ and $N^I_{K\kappa,K'\kappa'}$ are respectively the projected matrix elements of the Hamiltonian and the norm,

$$H^I_{K\kappa,K'\kappa'} = \langle\Phi_\kappa|\hat{H}\hat{P}^I_{KK'}|\Phi_{\kappa'}\rangle,\quad N^I_{K\kappa,K'\kappa'} = \langle\Phi_\kappa|\hat{P}^I_{KK'}|\Phi_{\kappa'}\rangle. \tag{6}$$

The large single-particle space with multiple major shells ensures that the collective motion and the cross-shell interplay are considered microscopically by the PSM. However, the shell-model dimension in Eq. (3) is not large, which means that each configuration in Eqs. (1) and (2) is a complex combination of the configurations constructed in the spherical shell-model basis. Thus, although the dimension of the configuration space in Eq. (3) where the final diagonalization is carried out is small, it is huge in the sense of conventional shell-model configurations. That is to say, the shell-model space is truncated efficiently in the PSM (see discussions in Ref. [27]).

B. The Hamiltonian

Following Ref. [30], the PSM Hamiltonian consists of the separable forces

$$\hat{H} = \hat{H}_0 + \hat{H}_{\rm QP} + \hat{H}_{\rm GT}, \tag{7}$$

which represent different kinds of correlations among valence nucleons. It has the single-particle terms $\hat{H}_0$, the quadrupole + pairing force $\hat{H}_{\rm QP}$, and the Gamow-Teller force of the charge-exchange terms, $\hat{H}_{\rm GT}$. $\hat{H}_0$ is the spherical single-particle term including the spin-orbit force. The second term, $\hat{H}_{\rm QP}$, contains three parts [28],

$$\hat{H}_{\rm QP} = -\frac{1}{2}\chi_{\rm QQ}\sum_\mu \hat{Q}^\dagger_{2\mu}\hat{Q}_{2\mu} - G_M\hat{P}^\dagger\hat{P} - G_Q\sum_\mu \hat{P}^\dagger_{2\mu}\hat{P}_{2\mu}, \tag{8}$$

which correspond to the quadrupole-quadrupole interaction, the monopole-pairing interaction, and the quadrupole-pairing interactions, respectively. The quadrupole + pairing force has been known to take care of basic correlations in nuclear structure, and it has been shown [46] that these interactions simulate the essence of the most important correlations in nuclei, so that any realistic forces have to contain at least these basic components implicitly in order to work successfully in structure calculations. The strength of the quadrupole-quadrupole term $\chi_{\rm QQ}$ is determined in a self-consistent manner so that it would give the empirical deformation of the basis as predicted in mean-field calculations [27,28]. The monopole-pairing strength is taken to be of the form $G_M = [G_1 \mp G_2(N-Z)/A]/A$, where "+" ("−") is for protons (neutrons), and N, Z, and A are the neutron number, proton number, and mass number, respectively. G_1 and G_2 are the coupling constants adjusted to yield the experimental odd-even mass differences in the corresponding nuclear mass region. The quadrupole-pairing strength is taken, as usual, to be about 20% of G_M [28,29]. It has been shown in many previous

publications that such a set of interactions can well describe detailed structures for well-deformed heavy nuclei [27].

The one-body operators in Eq. (8) are taken as the standard form

$$\begin{aligned}\hat{Q}_{2\mu} &= \sum_{\alpha,\alpha'}\langle\alpha|\hat{Q}_{2\mu}|\alpha'\rangle c^{\dagger}_{\alpha}c_{\alpha'},\\ \hat{P}^{\dagger} &= \frac{1}{2}\sum_{\alpha} c^{\dagger}_{\alpha}c^{\dagger}_{\bar{\alpha}},\\ \hat{P}^{\dagger}_{2\mu} &= \frac{1}{2}\sum_{\alpha,\alpha'}\langle\alpha|\hat{Q}_{2\mu}|\alpha'\rangle c^{\dagger}_{\alpha}c^{\dagger}_{\bar{\alpha}'},\end{aligned} \tag{9}$$

where $c^{\dagger}_{\alpha}$ (c_{α}) is the nucleon creation (annihilation) operator for the single-particle states in the spherical basis, and the quantum number $\alpha \equiv \{nljm\}$. The time reversal of c_{α} is defined as $c_{\bar{\alpha}} \equiv (-1)^{j-m}c_{nlj-m}$.

The last force, $\hat{H}_{\rm GT}$ in Eq. (7), is the two-body Gamow-Teller force:

$$\begin{aligned}\hat{H}_{\rm GT} = &+2\chi_{\rm GT}\sum_{\mu}\hat{\beta}^{-}_{1\mu}(-1)^{\mu}\hat{\beta}^{+}_{1-\mu}\\ &-2\kappa_{\rm GT}\sum_{\mu}\hat{\Gamma}^{-}_{1\mu}(-1)^{\mu}\hat{\Gamma}^{+}_{1-\mu}.\end{aligned} \tag{10}$$

This is a charge-dependent separable interaction with both particle-hole (p-h) and particle-particle (p-p) channels, which act between protons and neutrons. Such a type of force has been used by many authors in the study of single- and double-β decay [47–51]. The p-h and p-p interactions are repulsive and attractive, respectively, if we take positive values for the strength parameters $\chi_{\rm GT}$ and $\kappa_{\rm GT}$. The p-p interaction, which was introduced originally by Kuz'min and Soloviev [47], is a neutron-proton pairing force in the $J^{\pi} = 1^{+}$ channel. In this work, the interaction strengths are simply adopted as those in quasiparticle random phase approximation calculations for corresponding mass regions, i.e., $\chi_{\rm GT} = 0.10$, $\kappa_{\rm GT} = 0.05$ for medium-mass nuclei [51] and $\chi_{\rm GT} = 23/A$, $\kappa_{\rm GT} = 7.5/A$ for heavy nuclei [47]. We remark that, in the PSM framework, the parameters need to be carefully fitted by systematical studies as in Ref. [48].

The one-body operators in Eq. (10) are as follows:

$$\hat{\beta}^{-}_{1\mu} = \sum_{\pi,\nu}\langle\pi|\sigma_{\mu}\tau_{-}|\nu\rangle c^{\dagger}_{\pi}c_{\nu}, \qquad \hat{\beta}^{+}_{1\mu} = (-)^{\mu}(\hat{\beta}^{-}_{1-\mu})^{\dagger}, \tag{11}$$

$$\hat{\Gamma}^{-}_{1\mu} = \sum_{\pi,\nu}\langle\pi|\sigma_{\mu}\tau_{-}|\nu\rangle c^{\dagger}_{\pi}c^{\dagger}_{\bar{\nu}}, \qquad \hat{\Gamma}^{+}_{1\mu} = (-)^{\mu}(\hat{\Gamma}^{-}_{1-\mu})^{\dagger}, \tag{12}$$

where σ and τ are the Pauli spin operator and the isospin operator, respectively. It is mentioned here that the Hamiltonian in Eq. (7) may need to be extended when specific transition processes are studied. For example, the spin-dipole force would be necessary in calculation of first-forbidden transitions [48].

The probability of Gamow-Teller transition from an initial state ω of spin I_i to a final state ω' of spin I_f is defined as

$$B\left(\mathrm{GT}, I^{\omega}_{i} \to I^{\omega'}_{f}\right) = \frac{2I_f+1}{2I_i+1}\left|\left\langle\Psi^{\omega'}_{I_f}\|\hat{\beta}^{\pm}\|\Psi^{\omega}_{I_i}\right\rangle\right|^2. \tag{13}$$

C. Calculation procedure: Application of the Pfaffian method

Let us summarize briefly the logical structure of the PSM for B(GT) calculations. First, we diagonalize the matrix of Hamiltonian (7) in the projected basis (3) with the configuration spaces (1) and (2) for an odd-neutron and a corresponding odd-proton nucleus, respectively. This corresponds to solving the eigenvalue equation (5), from which one can obtain the spectra E^{ω}_{I} and the wave functions [given in terms of the coefficients $f^{\omega}_{IK_{\kappa}}$ in Eq. (3)] for two relevant odd-A nuclei. Then, a state-by-state calculation of the GT transition probability between the two odd-mass nuclei can be performed with Eq. (13) using the wave functions. From Eqs. (3), (4), (6), and (13), it is obvious that the central task in numerical calculations is to evaluate the rotated matrix elements of the Hamiltonian, the norm, and the one-body GT transition operator,

$$\begin{aligned}\mathcal{H}_{\kappa'\kappa} &= \langle\Phi_{\kappa'}(b)|\hat{H}[\Omega]|\Phi_{\kappa}(a)\rangle,\\ \mathcal{N}_{\kappa'\kappa} &= \langle\Phi_{\kappa'}(b)|[\Omega]|\Phi_{\kappa}(a)\rangle,\\ \mathcal{B}^{\pm}_{\kappa'\kappa} &= \langle\Phi_{\kappa'}(b)|\hat{\beta}^{\pm}_{1\mu}[\Omega]|\Phi_{\kappa}(a)\rangle,\end{aligned} \tag{14}$$

with the notation $[\Omega] = \hat{R}(\Omega)/\langle\Phi(b)|\hat{R}(\Omega)|\Phi(a)\rangle$ [28]. In the above expressions, (a) and (b) can represent states of the same nuclear system or different nuclear systems (e.g., a parent and a daughter nucleus), with corresponding qp creation (annihilation) operators $a^{\dagger}_{i}$ and $b^{\dagger}_{j}$ (a_i and b_j). In the following, we take $\mathcal{N}_{\kappa'\kappa}$ as an example to discuss the numerical procedure. Its explicit form can be written as

$$\mathcal{N}_{\kappa'\kappa} = \langle\Phi(b)|b_{1'}\cdots b_{n'}[\Omega]a^{\dagger}_{1}\cdots a^{\dagger}_{n}|\Phi(a)\rangle, \tag{15}$$

which is usually evaluated [28] by the generalized Wick theorem that decomposes Eq. (15) into a combination of three types of contraction, denoted as A, B, and C, with their matrix expressions [52]

$$\begin{aligned}A_{ij}(\Omega) &\equiv \langle\Phi(b)|[\Omega]a^{\dagger}_{i}a^{\dagger}_{j}|\Phi(a)\rangle = [V^{*}(\Omega)U^{-1}(\Omega)]_{ij},\\ B_{ij}(\Omega) &\equiv \langle\Phi(b)|b_j b_i[\Omega]|\Phi(a)\rangle = [U^{-1}(\Omega)V(\Omega)]_{ij},\\ C_{ij}(\Omega) &\equiv \langle\Phi(b)|b_i[\Omega]a^{\dagger}_{j}|\Phi(a)\rangle = [U^{-1}(\Omega)]_{ij},\end{aligned} \tag{16}$$

where U and V are the corresponding matrices of action of the rotation operator on quasiparticles [52]. It was pointed out [36] that, in applying the generalized Wick theorem, a matrix element of Eq. (15) involving n' and n qps, respectively on the left- and right-hand side of $[\Omega]$, contains $(n+n'-1)!!$ terms. In practice, the number of terms becomes so large that it is nearly impossible to write down expressions explicitly for more than four-qp states. In fact, the earlier version of the PSM configuration space for odd-mass nuclei was limited to one- and three-qp states [53,54].

By using the fermionic coherent state and Grassmann integral, it was shown that a general expression for the matrix elements (15) in terms of the Pfaffian can be derived as [36]

$$\begin{aligned}&\langle\Phi(b)|b_{1'}\cdots b_{n'}[\Omega]a^{\dagger}_{1}\cdots a^{\dagger}_{n}|\Phi(a)\rangle\\ &\quad = Pf(X) = Pf\begin{pmatrix} B & C\\ -C^{T} & A\end{pmatrix},\end{aligned} \tag{17}$$

where X is a skew-symmetric matrix with dimension $(n+n')\times(n+n')$. The indices of rows and columns for B run

from $1'$ to n' $(1',\ldots,n')$ and the ones for A run from 1 to n $(1,\ldots,n)$. For matrix C in Eq. (17), the indices of rows run from $1'$ to n' and those of columns run from 1 to n. The Pfaffian is defined as

$$Pf(\mathcal{A}) \equiv \frac{1}{2^n n!} \sum_{\sigma\in S_{2n}} \mathrm{sgn}(\sigma) \prod_{i=1}^{n} a_{\sigma(2i-1)\sigma(2i)} \tag{18}$$

for a skew-symmetric matrix $\mathcal{A}$ with dimension $2n \times 2n$, of which matrix elements are a_{ij}. The symbol σ is a permutation of $\{1,2,3,\ldots,2n\}$, $\mathrm{sgn}(\sigma)$ is its sign, and S_{2n} represents a symmetry group. This makes it possible and efficient to work with the expanded PSM configuration, since calculations of the corresponding Pfaffians are not time consuming [55].

III. RESULTS AND DISCUSSIONS

In the PSM, the standard Nilsson scheme [43] is used for generating deformed bases, and the Nilsson parameters, κ and μ, can be taken from the literature (e.g., Refs. [56,57]). The present computer code incorporates multiple shells, typically with two to four major harmonic-oscillation shells in the single-particle basis. This makes it possible to study GT transitions of highly excited states in a shell-model framework. In numerical calculations, we keep the axial symmetry in the deformed bases, which reduces D^I_{MK} in Eq. (4) to the small d function, and the three dimensions in Euler angles Ω are simplified to one (i.e., β). This reduces the numerical effort considerably.

A. The Ikeda sum rule

Before a new computer code for large-scale numerical calculations can be used, it is required to check carefully the correctness. In the content of the present study, the symmetry relations and normalization condition, as well as the well-known Ikeda sum rule [58], can be used to check numerical accuracy [30]. The employed symmetry relations between matrix elements and the normalization condition are

$$\begin{aligned} H^I_{K\kappa,K'\kappa'} &= H^I_{K'\kappa',K\kappa}, \\ N^I_{K\kappa,K'\kappa'} &= N^I_{K'\kappa',K\kappa}, \end{aligned} \tag{19}$$

$$\sum_{K\kappa K'\kappa'} f^{\omega}_{IK_\kappa} N^I_{K\kappa,K'\kappa'} f^{\omega}_{IK'_{\kappa'}} = 1, \tag{20}$$

$$\begin{aligned} \langle\Phi_{\kappa'}|\hat{\beta}^{\pm}_{1\mu}\hat{R}(\beta)|\Phi_\kappa\rangle &= (-)^{K_\kappa - K'_{\kappa'}} \sum_{\mu'} d^1_{\mu'-\mu}(\beta) \\ &\quad \times \langle\Phi_\kappa|\hat{\beta}^{\mp}_{1\mu'}\hat{R}(\beta)|\Phi_{\kappa'}\rangle, \end{aligned} \tag{21}$$

$$\langle\Psi_{I_f}\|\hat{\beta}^{\pm}\|\Psi_{I_i}\rangle = (-)^{I_f - I_i}\sqrt{\frac{2I_i+1}{2I_f+1}}\langle\Psi_{I_i}\|\hat{\beta}^{\mp}\|\Psi_{I_f}\rangle. \tag{22}$$

The fulfillment of the model-independent Ikeda sum rule [58] for GT transitions, expressed as

$$\begin{aligned} &S(\mathrm{GT}^-) - S(\mathrm{GT}^+) \\ &= \sum_f B(\mathrm{GT}^-, i \to f) - \sum_f B(\mathrm{GT}^+, i \to f) \\ &= 3(N-Z), \end{aligned} \tag{23}$$

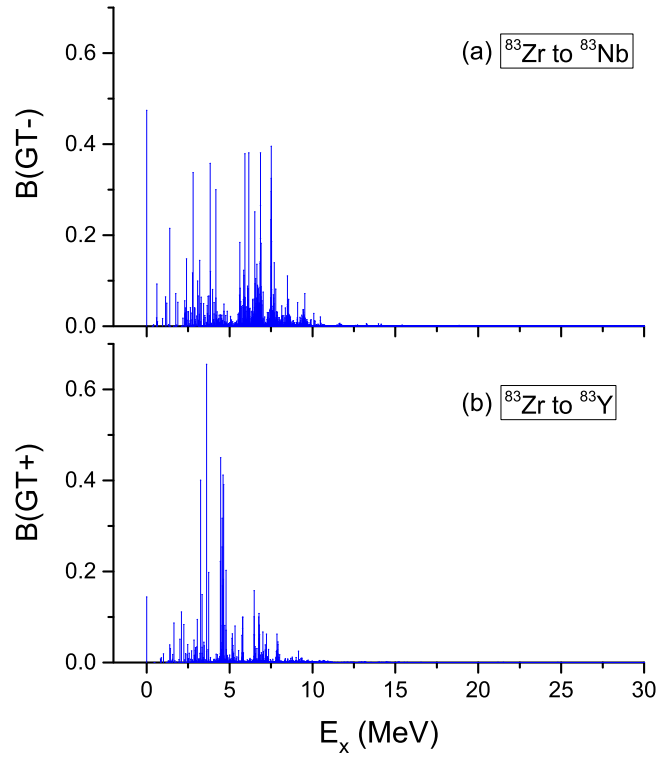

FIG. 1. The calculated GT strength distribution for $\beta^{\pm}$ transition from the first $1/2^-$ state of ^{83}Zr respectively to all $1/2^-$,$3/2^-$ states of (a) ^{83}Nb and (b) ^{83}Y, as a function of excitation energies.

is examined. The summations in Eq. (23) run over the complete sets of configurations of the final states constructed within the given model space. Since the basis of medium-heavy nuclei is relatively small, and thus it is easier to achieve completeness, we take the $A = 83$ nuclei as an example. The calculation involves $B(\mathrm{GT}^-, {}^{83}\mathrm{Zr} \to {}^{83}\mathrm{Nb})$ and $B(\mathrm{GT}^+, {}^{83}\mathrm{Zr} \to {}^{83}\mathrm{Y})$. In the numerical procedure, two major harmonic shells with $N = 3,4$ are used for both neutrons and protons, the quadrupole deformation for the bases is adopted as $\varepsilon_2 = 0.3$ for all three nuclei, and the strengths of the monopole-pairing interaction in Eq. (8) are taken as $G_1 = 20.25$ and $G_2 = 16.20$ [59]. The complete configuration spaces of each of the two daughter nuclei consist of about 7,000 one- and three-qp states.

In Fig. 1, we show the calculated $B(\mathrm{GT}^{\mp})$ from the first $1/2^-$ state of ^{83}Zr to all $1/2^-$,$3/2^-$ states of ^{83}Nb and ^{83}Y, respectively. It is seen that both $B(\mathrm{GT}^-)$ and $B(\mathrm{GT}^+)$ strengths are fragmented over many excited states, which can be visualized up to about 10 MeV in Fig. 1. $B(\mathrm{GT}^+)$ shows a peak located in 3–5 MeV. For the excitation region above 10 MeV, there are many tiny strengths in both plots, which decrease, roughly exponentially, towards the highest excitation in the calculation. Figure 2 illustrates these.

Adding up respectively all these $B(\mathrm{GT}^-)$ and $B(\mathrm{GT}^+)$ strengths, we get

$$S(\mathrm{GT}^-) = 19.3439, \quad S(\mathrm{GT}^+) = 10.4829, \tag{24}$$

which indicates that $S(\mathrm{GT}^-) - S(\mathrm{GT}^+)$ exhausts 98.5% of the sum-rule value $3(N-Z)$. Considering the fact that in our model, particle number is conserved at the BCS level, which

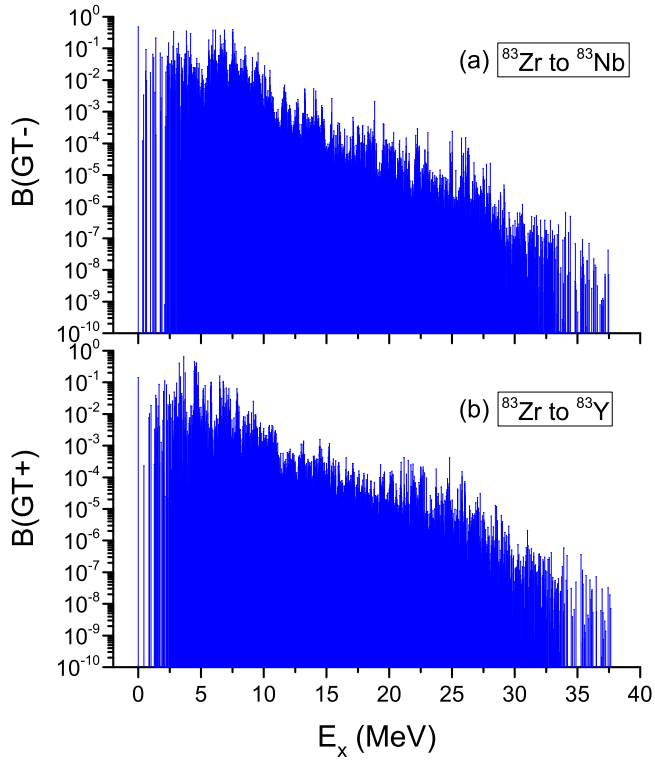

FIG. 2. Same as Fig. 1, but in logarithmic scale.

could be the source for the small violation of the total sum rule, the result can be considered satisfactory.

B. Example: GT transitions of ^{153}Nd → ^{153}Pm

We calculate β^--decay rates in neutron-rich rare-earth nuclei, from the parent nucleus ^{153}Nd to the daughter ^{153}Pm as our first example. It is well known that these two nuclei are well-deformed, axially symmetric nuclei. In the calculation, three major harmonic shells with $N = 4,5,6$ ($N = 3,4,5$) are taken for neutrons (protons) in heavy nuclei. The strengths of the monopole-pairing interaction in Eq. (8) are taken as $G_1 = 20.12$, $G_2 = 13.13$ [29]. The quadrupole and hexadecapole deformation parameters are adopted as $\varepsilon_2 = 0.250$ and $\varepsilon_4 = -0.073$ for both nuclei, taken from Ref. [60].

Before the model is applied for GT calculations, it is desirable to see how it describes the detailed nuclear structure and, in the first place, how well it can reproduce the known energy spectra for the relevant nuclei. In the case of ^{153}Nd, high-spin rotational bands are experimentally known up to about 3 MeV [61]. However, isomeric states are suggested to play crucial roles in understanding abundances of element production in the nucleosynthesis processes [40]. Recently, a rotational band based on the 1.17(7)-μs isomer at 191.7 keV was measured in ^{153}Nd [62]. This isomer was assigned a spin-parity of $5/2^+$. In the case of ^{153}Pm, structure data from experiment are presently scarce.

Figures 3 and 4 show, respectively, the calculated energy levels for ^{153}Nd and ^{153}Pm, which are compared with the available data [61,62]. It is seen that the PSM calculation can describe the structure data for the heavy deformed nuclei quantitatively. The spin and parity of the ground states for both nuclei are reproduced correctly, with $3/2^-$ for ^{153}Nd and $5/2^-$ for ^{153}Pm, respectively, in agreement with experimental data [61]. While in ^{153}Nd, the ground state has the main

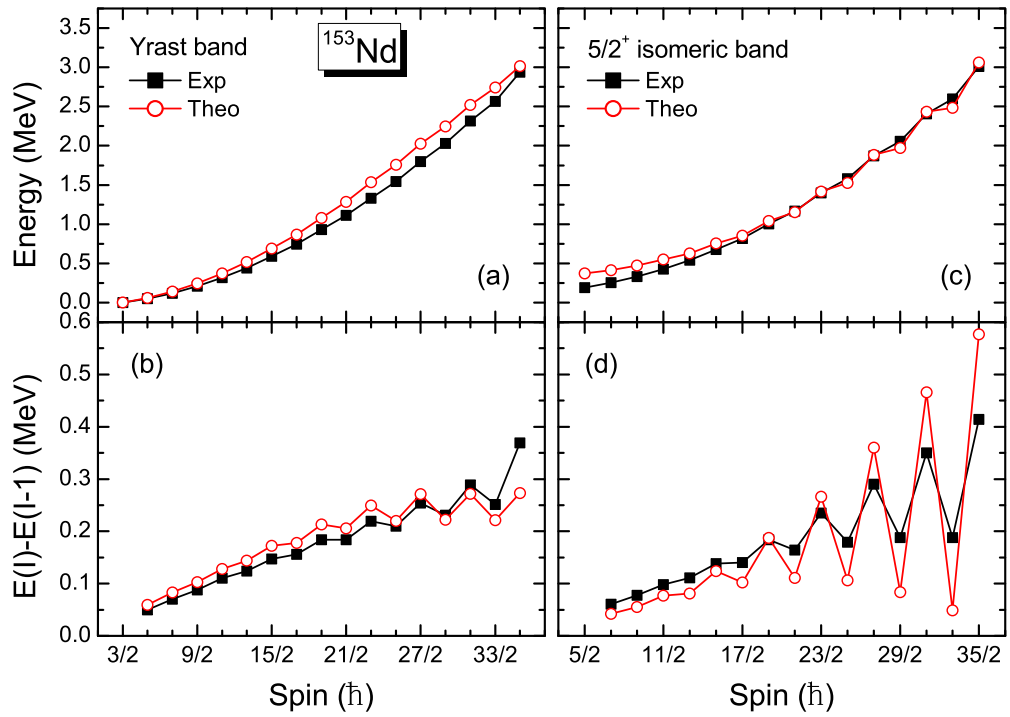

FIG. 3. (a) Calculated energies and (b) transition energies of the yrast band and (c) calculated energies and (d) transition energies of the band based on the 5/2 isomer for ^{153}Nd, as compared with the data taken from Refs. [61,62].

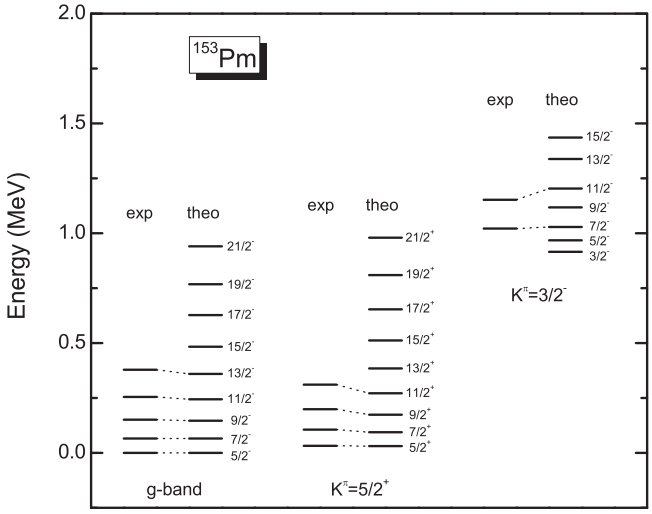

FIG. 4. Calculated energy levels of ^{153}Pm, as compared with the data taken from Ref. [61].

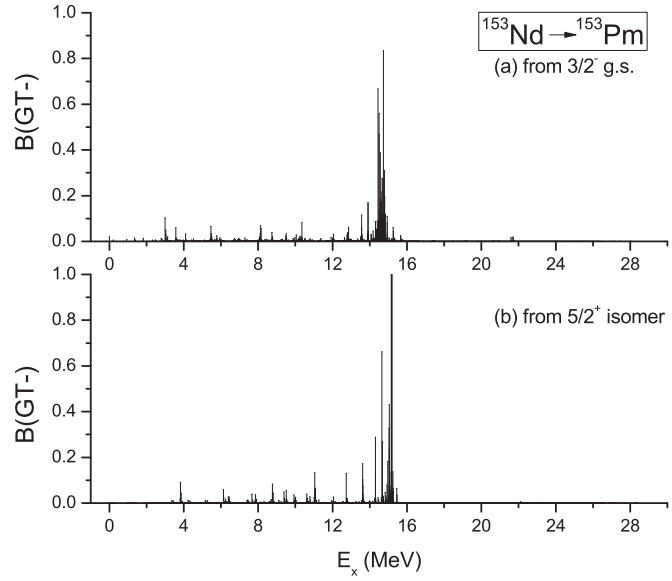

FIG. 5. Calculated GT strength distribution from the $3/2^-$ ground state and the $5/2^+$ isomeric state of ^{153}Nd to the excited states of ^{153}Pm.

configuration from the neutron Nilsson state $\nu 3/2^-[521]$ of the $\nu h_{9/2}$ orbit, that in ^{153}Pm has mainly the proton Nilsson state $\pi 5/2^-[532]$ of $\pi h_{11/2}$.

For the purpose of the present GT study, it is important that the model can describe excited states as well. It is our opinion that theoretical models that are used for GT calculations should be tested using existing structure data, particularly for those that are used to discuss GT transitions in thermal environments. For the ^{153}Nd calculation, the results in Fig. 3 are compared with known data [62] (basically of two high-spin rotational bands, one yrast band and one isomeric band based on the 1.17(7)-μs isomer), in the energy-spin type of plots for the sake of convenience. As shown in Fig. 3(b), the delicate zigzag behavior [which cannot be seen in Fig. 3(a) due to the scale] in the yrast band is described successfully, indicating the correct signature dependence [53] of this band. Figures 3(c) and 3(d) depict the energies and transition energies of the calculated $5/2^+$ isomeric bands, as compared with the data in Ref. [62]. It is seen that the calculated $5/2^+$ band can reproduce the data very well. A stronger zigzag behavior is seen in both experiment and calculation, although in the theoretical results, the calculated zigzag amplitude is somewhat larger. The main configuration of the bandhead is found to be $\nu 5/2^+[642]$, consistent with the suggestion in Ref. [62]. We note, in particular, that the two rotational bands in the discussion, though their bandheads are very close in energy (only less than 200 keV apart), have distinctive structure; in the first place, they belong to different parity groups. These make their GT strength distributions at the low-energy region very different, as we see below.

Experimental high-spin data for ^{153}Pm are presently rare. There are mainly known energy levels up to the $13/2^-$ state for the ground-state band starting from $3/2^-$ and those up to $11/2^+$ based on the $5/2^+$ state, all of which lie below 0.4 MeV in energy. As can be seen in Fig. 4, the PSM calculation describes these data reasonably well.

Now we turn the discussion to the calculated $B(\mathrm{GT}^-)$ values for the transition from the parent nucleus ^{153}Nd to the daughter ^{153}Pm. The discussion is divided into two different cases: GT transitions from the near-ground states of ^{153}Nd and those from the states of about 3.5 MeV of excitation in ^{153}Nd, essentially to all the allowed daughter states in ^{153}Pm up to 25 MeV. In the calculations, the configuration space of the daughter nucleus consists of about 15,000 positive-parity and negative-parity states, respectively.

Figure 5 shows the calculated $B(\mathrm{GT}^-)$ distribution from the $3/2^-$ ground state and the $5/2^+$ isomeric state of ^{153}Nd to the states of ^{153}Pm, as functions of excitation energies in ^{153}Pm. The main feature of the two plots in Fig. 5 is that the strengths are rather fragmented over many excited states but are clearly peaked in the energy range between 14 and 15 MeV. These peaks take most of the strengths, corresponding to a formation of the GT giant resonance. A giant resonance in nuclei is a collective behavior, which requires participation of many particles in the collective motion. That it appears in the calculation can be understood that in the PSM, each deformed nuclear state is a superposition of different qp configurations that consist of many deformed Nilsson orbitals, and each deformed Nilsson orbital is a superposition of many spherical orbits. Therefore, each PSM state is formed by complicated mixing of enormous configurations corresponding to the spherical basis [27].

Despite the complexity of the configuration mixing, it is possible to trace the dominant configurations of the states that contribute to the GT peaks in Fig. 5. This can be done by identifying them in the PSM wave functions in terms of the Nilsson notation [43]. In Table I, we list the dominant configurations of the states in ^{153}Pm around this peak to which the ground state of ^{153}Nd has large $B(\mathrm{GT}^-)$ values. It can be seen that although these configurations are three-qp states with different proton and neutron states, they all contain

TABLE I. Spins and dominant configurations for states in ^{153}Pm at $E_x \approx 15$ MeV to which the ^{153}Nd ground-state decay has large $B(\mathrm{GT}^-)$ values, corresponding to a GT giant resonance, as shown in Fig. 5(a).

Spin	K^π	Configuration
1/2	$1/2^-$	$\pi 3/2^-[541] \otimes \pi 3/2^-[532] \otimes \pi 5/2^-[532]$
1/2	$1/2^-$	$\pi 3/2^-[532] \otimes \pi 3/2^+[431] \otimes \pi 1/2^+[431]$
1/2	$1/2^-$	$\pi 3/2^-[541] \otimes \pi 1/2^+[431] \otimes \pi 3/2^+[402]$
3/2	$1/2^-$	$\pi 1/2^-[541] \otimes \nu 1/2^-[541] \otimes \nu 3/2^-[501]$
3/2	$3/2^-$	$\pi 1/2^-[541] \otimes \nu 5/2^-[532] \otimes \nu 3/2^-[512]$
5/2	$5/2^-$	$\pi 3/2^-[541] \otimes \pi 3/2^-[532] \otimes \pi 5/2^-[532]$
5/2	$1/2^-$	$\pi 5/2^-[532] \otimes \nu 3/2^-[532] \otimes \nu 3/2^-[512]$
5/2	$1/2^-$	$\pi 1/2^-[550] \otimes \nu 1/2^-[550] \otimes \nu 3/2^-[512]$
5/2	$5/2^-$	$\pi 5/2^-[523] \otimes \nu 3/2^-[541] \otimes \nu 3/2^-[521]$

one proton Nilsson orbit originating either from the $\pi h_{9/2}$ or from the $\pi h_{11/2}$ spherical orbit. This is simply because of the selection rule of allowed GT transition. As discussed before, the $3/2^-$ ground state of ^{153}Nd takes the neutron Nilsson state $\nu 3/2^-[521]$ as the main component, which originates from the $\nu h_{9/2}$ orbit of the spherical basis. Because the GT operators do not change the orbital angular momentum, as indicated in Eq. (11), transitions from the ^{153}Nd ground state to these ^{153}Pm daughter states should be strong.

Except for the giant resonance region, many other distributions with smaller GT strengths cannot be easily visualized in Fig. 5. Therefore, in Fig. 6, we re-plot them in the logarithmic scale. In Fig. 6(a), there is a group of discrete transitions up to 3 MeV, some of which have been known experimentally through the measured $\log(ft)$ values [61]. To compare our results with these data, we convert our theoretical GT transition rates to ft values by using

$$ft = \frac{6163.4}{\left(\frac{g_A}{g_V}\right)^2_{\mathrm{eff}} B(\mathrm{GT})}, \tag{25}$$

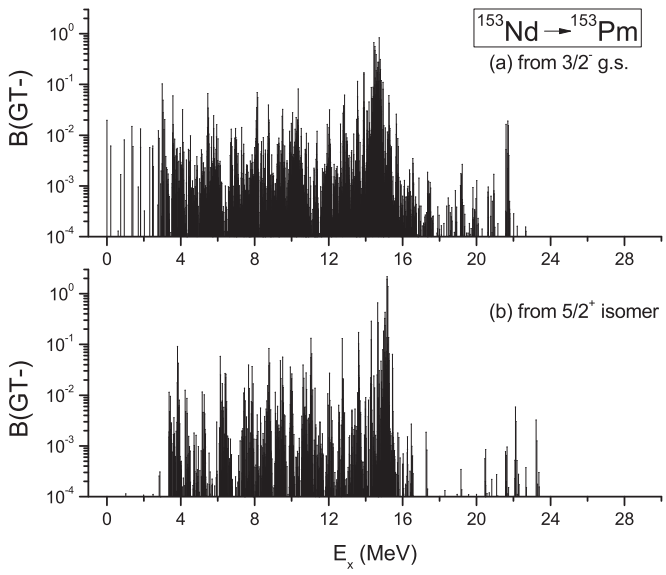

FIG. 6. Same as Fig. 5, but in logarithmic scale.

where ft is the comparative half-life, and the coupling constants in Ref. [63] are adopted as

$$\left(\frac{g_A}{g_V}\right)_{\mathrm{eff}} = 0.74\frac{g_A}{g_V}, \qquad \frac{g_A}{g_V} = -1.26. \tag{26}$$

In Table II, we list the $\log(ft)$ data taken from Ref. [61] and our calculations. Note that as the experiment could not identify the spin values of these states, it is difficult to make a direct comparison. For the theoretical values in Table II, we give a spin value of the daughter state for each transition, the excitation energy, the Nilsson K^π values, and the main configuration in the Nilsson notation. We can conclude that a qualitative agreement has been achieved, but warn that, except for the first five transitions to the daughter states with clear structures, we do not claim a one-to-one agreement with the rest of these experimental data.

We find that to reproduce the experimental $\log(ft)$ data (see Table II), an effective ratio of g_A/g_V is employed, corresponding to a quenching factor of 0.74, which is the same as that in Ref. [63] for single-shell shell-model calculations of the sd- and some pf-shell nuclei. For GT transition calculations, a quenching factor is usually introduced due to the model space limitation and missing degrees of freedom in the wave functions [64]. Very recently, the choice of the quenching factor for the axial coupling constant was discussed [65,66]. It is seen from the above results that, notwithstanding our large multishell model space, a quenching factor is still needed. This may indicate that our wave functions, with their relevant correlations mainly from Eq. (10), still lack some components. We note, nevertheless, that our employed value of 0.74 is larger than $A^{-0.12} = 0.547$ of the shell model [67]. It will be interesting to study systematically the configuration-space dependence of the g_A quenching factor within the PSM framework.

It is interesting to observe a remarkable difference between the two plots in Fig. 6. Despite their similarities in the GT distribution from 3.5 MeV up, it can be seen in Fig. 6(b) that transitions from the $5/2^+$ isomeric state in ^{153}Nd to the ^{153}Pm states are completely suppressed for the low-lying daughter states up to 3.5 MeV. This makes the GT transition from the two ^{153}Nd parent states, in spite of their being only less than 200 keV apart, very different. We can understand this remarkable difference by looking at the PSM wave functions. In the parent ^{153}Nd, the ground state corresponds to the Nilsson orbital $\nu 3/2^-[521]$ originating from $\nu h_{9/2}$, which is a normal state. However, the $5/2^+$ isomeric state corresponds to the Nilsson orbital $\nu 5/2^+[642]$ originating from $\nu i_{13/2}$, which is an abnormal (or intruder) state caused by the spin-orbit interaction. Although these two parent states lie nearly together in energy, it will be very different situations when they can find daughter states, to which they decay, having the same quantum number in orbital angular momentum. For the ^{153}Nd ground state, the daughter states in ^{153}Pm must have the main components from $\pi h_{9/2}$ or $\pi h_{11/2}$, among which, the Nilsson orbitals from $\pi h_{11/2}$ lie close to the proton Fermi surface in ^{153}Pm, and therefore, low-lying GT strengths can be formed, as discussed in Table II. In contrast, for the $5/2^+$ isomeric state in ^{153}Nd, the main structure is made of the intruder $\nu i_{13/2}$ state, and the daughter states in ^{153}Pm must have the main

TABLE II. Calculated energies, log(ft) values [extracted by using Eq. (25)], and dominant configurations for transitions from the ground state of ^{153}Nd to the low-lying states of ^{153}Pm, as compared with available data taken from Ref. [61].

Expt.			Theor.				
Spin	E (MeV)	log(ft)	Spin	E (MeV)	log(ft)	K^π	Configuration
5/2	0	5.39	5/2	0	5.55	$5/2^-$	$\pi 5/2^-[532]$
	0.967	6.38	5/2	0.945	6.05	$5/2^-$	$\pi 5/2^-[532] \otimes \nu 3/2^+[651] \otimes \nu 3/2^+[651]$
	1.296	6.19	5/2	1.411	6.07	$3/2^-$	$\pi 3/2^-[541]$
	1.732	6.30	1/2	1.699	6.77	$1/2^-$	$\pi 1/2^-[550]$
	1.776	6.38	3/2	1.810	6.12	$1/2^-$	$\pi 1/2^-[550]$
	1.838	6.12	5/2	1.829	5.97	$5/2^-$	$\pi 5/2^-[532] \otimes \nu 3/2^-[521] \otimes \nu 3/2^-[521]$
	1.851	6.19	5/2	2.126	6.09	$5/2^-$	$\pi 5/2^-[532] \otimes \nu 5/2^+[642] \otimes \nu 5/2^+[642]$
	1.988	5.57	5/2	2.586	5.76	$3/2^-$	$\pi 5/2^-[532] \otimes \nu 3/2^+[651] \otimes \nu 5/2^+[642]$
	1.998	5.10	5/2	2.598	4.99	$5/2^-$	$\pi 5/2^-[532] \otimes \nu 3/2^-[532] \otimes \nu 3/2^-[521]$
	2.005	5.28	1/2	2.701	5.16	$1/2^-$	$\pi 5/2^-[532] \otimes \nu 3/2^-[532] \otimes \nu 3/2^-[521]$
	2.008	6.16	5/2	2.712	6.46	$5/2^-$	$\pi 5/2^-[532] \otimes \pi 3/2^+[411] \otimes \pi 3/2^+[411]$
	2.033	5.69	3/2	2.721	5.41	$1/2^-$	$\pi 5/2^-[532] \otimes \nu 3/2^-[532] \otimes \nu 3/2^-[521]$
	2.035	6.11	3/2	2.757	6.67	$3/2^-$	$\pi 5/2^-[532] \otimes \nu 1/2^+[660] \otimes \nu 3/2^+[651]$
	2.061	6.02	5/2	2.760	5.94	$1/2^-$	$\pi 5/2^-[532] \otimes \nu 3/2^-[532] \otimes \nu 3/2^-[521]$

components from $\pi i_{11/2}$ or $\pi i_{13/2}$, among which, $\pi i_{11/2}$ is out of the question because it lies far above the $N = 126$ major shell gap. The isomer decay to the states in ^{153}Pm with $\pi i_{13/2}$ as components is possible, but because the Nilsson orbitals originating from $\pi i_{13/2}$ are not near the proton Fermi surface in ^{153}Pm, the strength can appear only starting from some excitations, roughly from 3.5 MeV in this case.

Our next discussion about the transition from the parent nucleus ^{153}Nd to the daughter ^{153}Pm regards the calculated $B(\mathrm{GT}^-)$ values initially from the excited states of the parent. Somewhat arbitrarily, we choose to study two $3/2^-$ excited states in ^{153}Nd, from which we calculate GT transition rates to all possible states in ^{153}Pm. The two $3/2^-$ states lie very close in energy, one at 3.45 MeV with the three-qp configuration $\nu 5/2^-[523] \otimes \pi 3/2^+[422] \otimes \pi 3/2^+[411]$ with $K^\pi = 1/2^-$ and the other at 3.67 MeV with $\nu 3/2^+[651] \otimes \nu 3/2^-[521] \otimes \nu 5/2^+[642]$ with $K^\pi = 3/2^-$. Although they are close in energy, notably they have very different structures; the 3.45-MeV one contains in its structure the last neutron originating from the $\nu f_{7/2}$ orbit with $l = 3$ and the 3.67-MeV one has the last neutron from the $\nu i_{13/2}$ with $l = 6$. Figure 7 shows the calculated results for GT transitions from these two states.

Very different patterns can be seen in the two plots of Fig. 7. In Fig. 7(a) the strengths are found mainly in the energy region from 4 to 12 MeV, among which there are essentially no strengths larger than 0.1. In a completely different picture, those in Fig. 7(b) are more fragmented, starting from low-lying states with a clear GT peak around 15 MeV, with some strengths reaching 1.0. The pattern of Fig. 7(b) (GT transitions from the $3/2^-$ state at 3.67 MeV) looks similar to that of Fig. 6(b), at least for the large excitation region from 4 to 16 MeV. This similarity can be understood because in both cases, the initial parent states in ^{153}Nd contain the last neutron state from the $\nu i_{13/2}$ spherical orbit. In contrast, for the results in Fig. 7(a), strong strengths cannot be formed in the energy range from 12 to 16 MeV, simply because of the shell structure. In the deformed single-particle picture, the proton states with $l = 3$ (i.e., $\pi f_{5/2}$ and $\pi f_{7/2}$) that can have large GT matrix elements with the neutron state $\nu 5/2^-[523]$ lie very far above the proton $N = 82$ shell. Therefore, strong transitions may exist, but must lie far above the energy range as presented in Fig. 7.

Most future applications by the present method imply an environment of finite temperature, notably in stellar scenarios. Therefore, GT rates of initially excited states become relevant. Contributions of the excited states are usually estimated by applying the generalized Brink-Axel (BA) hypothesis [26], which states essentially that the rates are independent of the properties of the initial and final states. While the validity of the Brink-Axel hypothesis in the GT channel has not been systematically checked for heavy deformed mass regions, our results in Fig. 7 at least suggest that it should be taken with great care. It is also worthy to mention that for astrophysical

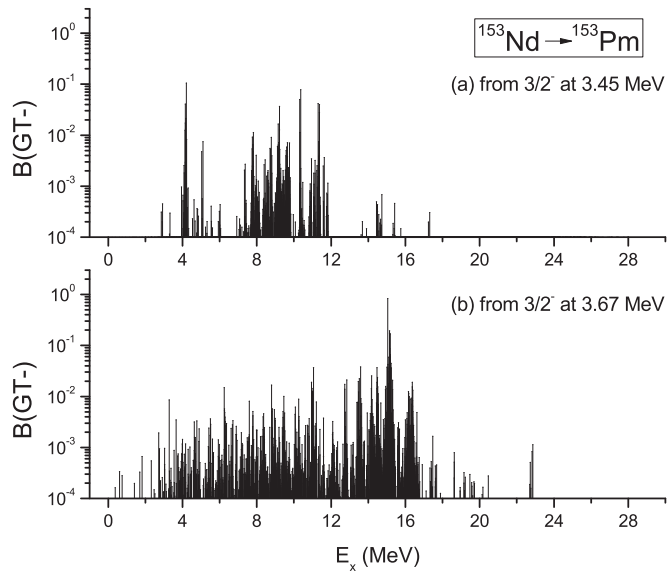

FIG. 7. Calculated GT strength distribution from two $3/2^-$ states of ^{153}Nd at about 3.5 MeV to the excited states of ^{153}Pm.

simulations the phenomenological approach of β-decay gross theory [68] is often applied due to lack of both experimental and microscopic theoretical values. It is well known that the gross theory failed to describe the complex nature of β decay as well as fine nuclear structure. As shown in the present study, the GT strength distribution sensibly depends on the underlying fine nuclear structure of involved nuclei; the microscopic approach employed here will be helpful to reduce uncertainties related to GT transition in heavy deformed nuclei.

IV. SUMMARY

To summarize, a qualitative description of GT transitions for heavy deformed odd-mass nuclei has been a challenge for theoretical models. It is particularly difficult to calculate in detail the state-to-state transitions for high excitations including the region where GT giant resonances appear. The present work is devoted to a new development of the shell-model method within the framework of the projected shell model for calculating GT transition rates. To achieve the numerical requirement, the Pfaffian algorithm has been used in the computation.

β^- decays from heavy deformed neutron-rich ^{153}Nd to ^{153}Pm are investigated as the first example. We showed that the experimentally known GT transition strengths from the ground state of ^{153}Nd to the low-lying states of ^{153}Pm can be reasonably well reproduced. Most of our discussions have been concentrated on the transition distributions from different initial states, including the ground state, the low-energy isomeric state, and the moderately high excited states but with different structures. It was found that, for deformed nuclei, GT transitions are in general strongly state dependent. We gave detailed explanations based on their relevant structure as to why the particular GT distribution patterns should occur. The initial results tend to indicate that both the shell effect determined by the spin-orbit interaction and the deformation effect, the two basic concepts that have governed the entire microscopic discussions in nuclear structure physics, are the key ingredients. The results presented here support the predictive power of the PSM for calculating GT strength for the nuclei which are extremely challenging from an experimental point of view. Further work towards a better understanding is in progress.

ACKNOWLEDGMENTS

The authors thank Z.-C. Gao for valuable discussions. Research at Shanghai Jiao Tong University is supported by the National Natural Science Foundation of China (Grant No. 11575112) and by the National Key Program for S&T Research and Development (Grant No. 2016YFA0400501).

[1] G. M. Fuller, W. A. Fowler, and M. J. Newman, Astrophys. J. Suppl. **42**, 447 (1980).
[2] G. M. Fuller, W. A. Fowler, and M. J. Newman, Astrophys. J. **252**, 715 (1982).
[3] G. M. Fuller, W. A. Fowler, and M. J. Newman, Astrophys. J. Suppl. **48**, 279 (1982).
[4] G. M. Fuller, W. A. Fowler, and M. J. Newman, Astrophys. J. **293**, 1 (1985).
[5] G. W. Misch and G. M. Fuller, Phys. Rev. C **94**, 055808 (2016).
[6] G. W. Misch, Astrophys. J. **844**, 20 (2017).
[7] G. W. Misch, Y. Sun, and G. M. Fuller, Astrophys. J. **852**, 43 (2018).
[8] K. Langanke and G. Martínez-Pinedo, Rev. Mod. Phys. **75**, 819 (2003).
[9] H.-Th. Janka, K. Langanke, A. Marek, G. Martínez-Pinedo, and B. Müller, Phys. Rep. **442**, 38 (2007).
[10] A. L. Cole, T. S. Anderson, R. G. T. Zegers, S. M. Austin, B. A. Brown, L. Valdez, S. Gupta, G. W. Hitt, and O. Fawwaz, Phys. Rev. C **86**, 015809 (2012).
[11] G. W. Misch, G. M. Fuller, and B. A. Brown, Phys. Rev. C **90**, 065808 (2014).
[12] F. T. Avignone III, S. R. Elliott, and J. Engel, Rev. Mod. Phys. **80**, 481 (2008).
[13] C. J. Guess, T. Adachi, H. Akimune, A. Algora, S. M. Austin, D. Bazin, B. A. Brown, C. Caesar, J. M. Deaven, H. Ejiri, E. Estevez, D. Fang, A. Faessler, D. Frekers, H. Fujita, Y. Fujita, M. Fujiwara, G. F. Grinyer, M. N. Harakeh, K. Hatanaka, C. Herlitzius, K. Hirota, G. W. Hitt, D. Ishikawa, H. Matsubara, R. Meharchand, F. Molina, H. Okamura, H. J. Ong, G. Perdikakis, V. Rodin, B. Rubio, Y. Shimbara, G. Süsoy, T. Suzuki, A. Tamii, J. H. Thies, C. Tur, N. Verhanovitz, M. Yosoi, J. Yurkon, R. G. T. Zegers, and J. Zenihiro, Phys. Rev. C **83**, 064318 (2011).
[14] C.-B. Fu *et al.*, Sci. Bull. **60**, 1211 (2015).
[15] X. Zhang, J. Zhao, D. Yuan, C. Fu, J. Bao, L. Chen, J. He, L. Hou, L. Li, Y. Li, Y. Li, G. Liao, Y. Rhee, Y. Sun, S. Xu, G. Zhao, B. Zhu, J. Zhu, Z. Zhang, and J. Zhang, Phys. Rev. C **96**, 055801 (2017).
[16] Y. Fujita, B. Rubio, and W. Gelletly, Prog. Part. Nucl. Phys. **66**, 549 (2011).
[17] F. Osterfeld, Rev. Mod. Phys. **64**, 491 (1992).
[18] N. Ryezayeva *et al.*, Phys. Lett. B **639**, 623 (2006).
[19] S. Rakers *et al.*, Nucl. Instrum. Methods Phys. Res. Sect. A **481**, 253 (2002).
[20] M. B. Aufderheide, S. D. Bloom, D. A. Resler, and G. J. Mathews, Phys. Rev. C **47**, 2961 (1993).
[21] E. Caurier, G. Martínez-Pinedo, F. Nowacki, A. Poves, and A. P. Zuker, Rev. Mod. Phys. **77**, 427 (2005).
[22] B. H. Wildenthal, Prog. Part. Nucl. Phys. **11**, 5 (1984).
[23] B. A. Brown and B. H. Wildenthal, At. Data Nucl. Data Tables **33**, 347 (1985).
[24] T. Oda *et al.*, At. Data Nucl. Data Tables **56**, 231 (1994).
[25] K. Langanke and G. Martínez-Pinedo, At. Data Nucl. Data Tables **79**, 1 (2001).
[26] D. M. Brink, Ph.D. thesis, Oxford University, 1955; P. Axel, Phys. Rev. **126**, 671 (1962).
[27] Y. Sun, Phys. Scr. **91**, 043005 (2016).
[28] K. Hara and Y. Sun, Int. J. Mod. Phys. E **4**, 637 (1995).
[29] Y. Sun and D. H. Feng, Phys. Rep. **264**, 375 (1996).
[30] Z.-C. Gao, Y. Sun, and Y.-S. Chen, Phys. Rev. C **74**, 054303 (2006).
[31] G. Mention, M. Fechner, T. Lasserre, T. A. Mueller, D. Lhuillier, M. Cribier, and A. Letourneau, Phys. Rev. D **83**, 073006 (2011).
[32] F. P. An *et al.*, Phys. Rev. Lett. **116**, 061801 (2016).
[33] A. A. Sonzogni, T. D. Johnson, and E. A. McCutchan, Phys. Rev. C **91**, 011301(R) (2015).

[34] L. M. Robledo, Phys. Rev. C **79**, 021302(R) (2009).
[35] G. F. Bertsch and L. M. Robledo, Phys. Rev. Lett. **108**, 042505 (2012).
[36] T. Mizusaki, M. Oi, F. Q. Chen, and Y. Sun, Phys. Lett. B **725**, 175 (2013).
[37] L.-J. Wang, F.-Q. Chen, T. Mizusaki, M. Oi, and Y. Sun, Phys. Rev. C **90**, 011303(R) (2014).
[38] L.-J. Wang, Y. Sun, T. Mizusaki, M. Oi, and S. K. Ghorui, Phys. Rev. C **93**, 034322 (2016).
[39] M. Lugaro *et al.*, Science **345**, 650 (2014).
[40] A. Aprahamian and Y. Sun, Nat. Phys. **1**, 81 (2005).
[41] Y. Sun, M. Wiescher, A. Aprahamian, and J. Fisker, Nucl. Phys. A **758**, 765 (2005).
[42] Y. Sun, X.-R. Zhou, G.-L. Long, E.-G. Zhao, and P. M. Walker, Phys. Lett. B **589**, 83 (2004).
[43] S. G. Nilsson *et al.*, Nucl. Phys. A **131**, 1 (1969).
[44] P. Ring and P. Schuck, *The Nuclear Many-Body Problem* (Springer-Verlag, Berlin, 2004).
[45] D. A. Varshalovich, A. N. Moskalev, and V. K. Khersonskii, *Quantum Theory of Angular Momentum* (World Scientific, Singapore, 1988).
[46] M. Dufour and A. P. Zuker, Phys. Rev. C **54**, 1641 (1996).
[47] V. A. Kuz'min and V. G. Soloviev, Nucl. Phys. A **486**, 118 (1988).
[48] H. Homma, E. Bender, M. Hirsch, K. Muto, H. V. Klapdor-Kleingrothaus, and T. Oda, Phys. Rev. C **54**, 2972 (1996).
[49] J. Suhonen and O. Civitarese, Phys. Rep. **300**, 123 (1998).
[50] O. Moreno *et al.*, Prog. Part. Nucl. Phys. **57**, 254 (2006).
[51] P. Sarriguren, Phys. Rev. C **87**, 045801 (2013).
[52] K. Hara and S. Iwasaki, Nucl. Phys. A **332**, 61 (1979).
[53] K. Hara and Y. Sun, Nucl. Phys. A **537**, 77 (1992).
[54] K. Hara and Y. Sun, Comput. Phys. Commun. **104**, 245 (1997).
[55] C. González-Ballestero, L. M. Robledo, and G. F. Bertsch, Comput. Phys. Commun. **182**, 2213 (2011).
[56] T. Bengtsson and I. Ragnarsson, Nucl. Phys. A **436**, 14 (1985).
[57] A. K. Jain, R. K. Sheline, P. C. Sood, and K. Jain, Rev. Mod. Phys. **62**, 393 (1990).
[58] K. Ikeda, T. Udagawa, and H. Yamaura, Prog. Theor. Phys. **33**, 22 (1965).
[59] Y.-X. Liu, Y. Sun, X.-H. Zhou, Y.-H. Zhang, S.-Y. Yu, Y.-C. Yang, and H. Jin, Nucl. Phys. A **858**, 11 (2011).
[60] P. Möller, J. R. Nix, W. D. Myers, and W. J. Swiatecki, At. Data Nucl. Data Tables **59**, 185 (1995).
[61] R. G. Helmer, Nucl. Data Sheets **107**, 507 (2006).
[62] G. S. Simpson, W. Urban, J. A. Pinston, J. C. Angelique, I. Deloncle, H. R. Faust, J. Genevey, U. Köster, T. Materna, R. Orlandi, A. Scherillo, A. G. Smith, J. F. Smith, T. Rząca-Urban, I. Ahmad, and J. P. Greene, Phys. Rev. C **81**, 024313 (2010).
[63] K. Langanke and G. Martínez-Pinedo, Nucl. Phys. A **673**, 481 (2000).
[64] N. Yoshida and F. Iachello, Prog. Theor. Exp. Phys. (2013) 043D01.
[65] J. T. Suhonen, Front. Phys. **5**, 55 (2017).
[66] J. Suhonen, Phys. Rev. C **96**, 055501 (2017).
[67] J. Barea, J. Kotila, and F. Iachello, Phys. Rev. C **87**, 014315 (2013).
[68] H. Koura, T. Tachibana, M. Uno, and M. Yamada, Prog. Theor. Phys. **113**, 305 (2005).